Kinks in chains with on-site bistable nondegenerate potential: Beyond traveling waves

I. B. Shiroky and O. V. Gendelman*
Faculty of Mechanical Engineering, Technion, Haifa 32000, Israel

(Received 25 October 2017; revised manuscript received 31 May 2018; published 31 July 2018)

This paper revisits the well-known transition fronts (kinks) in chains of coupled oscillators with nondegenerate on-site potentials. Usually, such transition fronts are considered in terms of traveling-wave solutions. We explore the loss of stability of such traveling waves. Generically, it corresponds to one of the common scenarios for fixed points of discrete maps. For example, one can encounter the quasiperiodic kink propagation (due to Hopf bifurcation), or the Feigenbaum cascade of period doublings, leading to a chaoticlike propagation pattern. The aforementioned scenarios show up, for instance, for triparabolic and φ^4 on-site potentials. Numeric evidence suggests that the loss of stability occurs due to resonances between the frequency associated with the kink propagation, and the linear band gaps of the chain. Particular resonance mechanisms are model dependent. For the classical Atkinson-Cabrera model with a biparabolic on-site potential, the stability threshold is estimated by the simple means of linear algebra. The loss of stability in this model occurs through Hopf bifurcation. The results are in good agreement with numerical simulations.

DOI: 10.1103/PhysRevE.98.012220

I. INTRODUCTION

Lattice models of mobile defects and transition fronts (kinks) are ubiquitous in physics. The idea dates back to a seminal work of Frenkel and Kontorova (FK model), who used a discrete variant of the sine-Gordon equation to describe the motion of dislocations [1]. Atkinson and Cabrera [2] replaced the sinusoidal potential with a simplified piecewise parabolic one to obtain analytically solvable equations for the original discrete lattice. A variant of the FK model with a triple-parabola potential was adopted for twinning dislocations in [3]. A similar model was further used to describe transition between dynamical phases, unlocking transitions, and Aubry transitions in Josephson junction arrays [4]. In [5], Truskinovsky and Vainchtein used the model with piecewise linear interparticle forcing to analyze martensitic phase transitions. Among other applications, one encounters detonation of primary explosives, domain walls in ferroelectrics [6], cracks in metals [7,8], lattice distortion around twin boundaries [9], dry friction [10], statistical mechanics [11], crowdions in anisotropic crystals [12], motion of fronts in semiconductor superlattices [13], dynamics of carbon nanotube foams [14], interaction of nonrigid walls in double-walled carbon nanotubes [15], superionic conductors [16], calcium release in cells [17], and others [18].

Propagating transition fronts in the bistable medium are usually explored as traveling waves [2,5,19–21]. It is commonly believed that in such models the front propagation velocity is uniquely defined by the system parameters. In linear chains with a piecewise parabolic on-site potential, above a certain threshold of the energetic gain at each site (or, equivalently, constant external forcing), the solution satisfies an "admissibility condition," meaning that at each instance the chain is separated into two continuous segments; one is placed within the metastable well and the other within the stable one [21,3]. Under this assumption, the model is solvable analytically, and one can obtain the unique velocity of the kink propagation. The consequent relation between the applied stress and the velocity of propagation, called the "kinetic relation," consists of segments separated by resonant velocities. It turns out that all the segments below the highest of resonant velocities actually violate the assumed admissibility condition and have to be removed due to inconsistency with the admissible traveling-wave solution. It is important to notice that the existence of "admissible traveling waves" does not imply their stability. Rather, the traveling waves lose stability above the first resonant velocity [19,22,23].

For linear chains with a smooth nondegenerate bistable on-site potential, the analytical solution is not available. However, numerical studies and asymptotic analytical approximations indicate, in most cases, qualitatively similar behavior [19–21]. The stability of a driven topological soliton in a Frenkel-Kontorova model in the so-called "fast region" has been studied by Braun *et al.* [24]. In the underdamped case, the solution loses stability by appearance of a discrete breather within the tail. Recent studies devoted to the effect of nonlinear interparticle interactions [25,20], demonstrated that in these cases the propagation of the traveling-wave fronts is dominated mostly by the nonlinearity, if the latter is strong enough. In this case, the traveling fronts propagate in the form of shock waves and reach very large energy concentration and far supersonic velocity, and primarily depend only on general shape characteristics of the on-site potential, rather than on its fine details. Other studies [26,27], which also address the case of generic coupling with on-site damping, propose a relation between the transported kinetic energy, the dissipation ratio, and the velocity.

Much less is known about the propagation of transition fronts for the parameter region that does not allow the admissibility conditions to be satisfied. This could happen for

*ovgend@technion.ac.il

low values of the energetic gain, where the front moves relatively slowly, and its velocity falls below the maximum group velocity of the linear substructure of the chain [28]. For the Atkinson-Cabrera model, below a certain threshold, traveling waves do not exist in this case [2,3,19,21,22]. This conclusion motivated studies that tried to construct solutions in the "problematic" region. Vainchtein in [3] implements an analytical approach proposed by Flytzanis *et al.* [29] to study a generalization of the Atkinson-Cabrera model. In this model, the two convex parabolas are connected by a concave one (a spinodal region) and form a continuously differentiable function. If the spinodal region is wide enough, solutions with more complex structure are stable. Specifically, solutions with low velocities are stable and emit waves in both directions. Similar results were also observed by Peyrard and Kruskal [30] and Earmme and Weiner [22]. Another interesting observation, obtained numerically, is that by implementing a fully nonlinear potential, the slow solutions are further stabilized. The authors of [23] focus on the degenerate case of [3], where the spinodal region is with zero width, or equivalently the Atkinson-Cabrera model. By applying a similar analytical approach, new solutions, which apparently complete the gap where the basic admissibility conditions are violated, are constructed. However, numerical simulations indicate that these solutions are unstable. Therefore, it seems that the basic piecewise parabolic model cannot be applied to describe slow propagation of dislocations. In [31] a trilinear nearest-neighbor interaction is considered and is also solved by applying the technique of [29]. As the spinodal region is increased, one encounters solutions that emit waves of different frequencies in both directions, and a kinetic relation with several segments separated by velocity gaps.

At the same time, as previously noted, even if the admissibility conditions are satisfied (put simply, the kink velocity exceeds the maximum linear group velocity in the system), it does not mean that such traveling-wave propagating front will be stable. The propagating front can have more complicated structure than the one enforced by the traveling-wave ansatz. For instance, rich patterns of possible front propagation were observed in continuous models of detonation waves based on the Burgers equation. The authors of [32] propose an extension of the Fickett model [33] to describe a chemical reaction with an induction zone followed by a heat release zone. These models yield pulsating and even chaotic propagating solutions. In [34], a model that predicts a shock wave in detonation in chemical mixtures is considered. Although this model is a very simple scalar first order partial differential equation, it is rich enough to produce instability and chaos through the classical sequence of period doublings.

In discrete lattices such kinks, that are *not* traveling waves, are less known and less explored. However, from general considerations, they should be ubiquitous in the chain models with appropriate structure. The reason is that the problem of the front propagation may be reformulated as a nonlinear map, and the traveling-wave solution corresponds to the fixed point of this map. When the parameters vary, such fixed points can lose stability through generic and well-known bifurcation scenarios [35,36]. After such bifurcations, one expects to observe stable propagating fronts that do not obey the traveling-wave ansatz. In the current paper, we describe such kinks for two benchmark models and illustrate physical mechanisms underlying the loss of stability of the traveling waves.

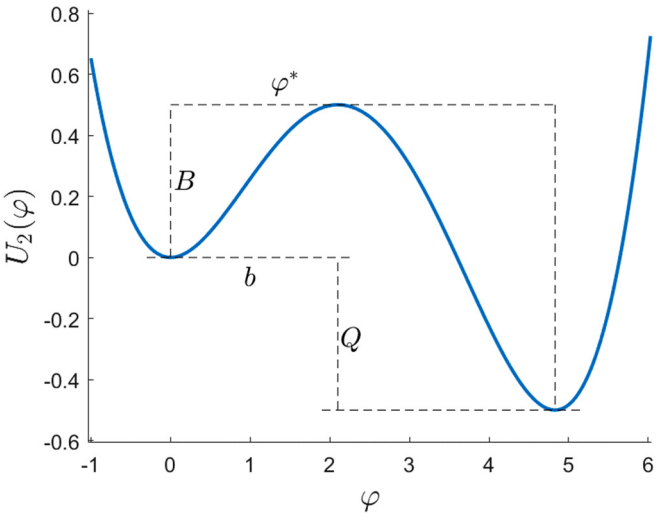

FIG. 1. A generic on-site bistable potential $U_2(\varphi)$.

II. DESCRIPTION OF THE GENERAL MODEL

To illustrate the general idea, we consider a common chain of oscillators with a smooth nearest-neighbor coupling potential $U_1(\varphi_n - \varphi_{n+1})$ subject to a bistable on-site potential $U_2(\varphi_n)$. The chain is described by the following set of equations:

$$\ddot{\varphi}_n + U_1'(\varphi_n - \varphi_{n+1}) + U_1'(\varphi_n - \varphi_{n-1}) + \xi\dot{\varphi}_n = -U_2'(\varphi_n). \tag{1}$$

φ_n is the displacement of the nth particle from the initial equilibrium state meta-stable); ξ is the linear on-site damping coefficient. The mass of each particle is set to unity.

The generic on-site potential U_2 is characterized by the energetic effect Q, the height of the potential barrier B, the coordinate of the barrier b, and the coordinate of the stable state φ^*, as illustrated in Fig. 1. The condition for nondegeneracy of the potential is $Q > 0$.

We consider the propagation of a general transition front (not necessarily a traveling wave) and therefore assume that every particle passes for the first time from the metastable to the stable well in successive order. Each particle passes the barrier for the first time at certain time instance t_k: $\varphi_k(t_k) = b, t_i < t_j \forall i < j; i, j \in \mathbb{Z}$. Without loss of generality we set $t_0 = 0$. The state vector is defined as follows:

$$\bar{X}(t) = \begin{pmatrix} \bar{\Phi} \\ \bar{V} \end{pmatrix}, \quad \bar{\Phi} = \begin{pmatrix} \vdots \\ \varphi_{n-1}(t) \\ \varphi_n(t) \\ \varphi_{n+1}(t) \\ \vdots \end{pmatrix}, \quad \bar{V} = \frac{d\bar{\Phi}}{dt}. \tag{2}$$

Then, if one denotes $\bar{X}_k = \bar{X}(t_k)$, then $\bar{X}_k$ constitutes a complete set of initial conditions for system (1) at time instance $t = t_k$. Therefore, it defines the state of the system when the next particle will cross the barrier for the first time. Formally,

this obvious fact can be written down as a formal smooth map:

$$\bar{X}_{k+1} = \mathbf{F}(\bar{X}_k). \tag{3}$$

Then, we define an invertible "shift backwards" operator acting on $\bar{X}(t)$ as follows:

$$\hat{S}(\bar{X}) = \begin{pmatrix} \bar{Q} \\ \bar{P} \end{pmatrix}, \quad q_n = \varphi_{n+1}, \quad \bar{P} = \frac{d\bar{Q}}{dt}. \tag{4}$$

A similar idea with the introduction of the cyclic shift matrix was used for stability analysis of the kink in a driven Frenkel-Kontorova chain with periodic boundary conditions [24,37]. We introduce an auxiliary variable $\bar{Y}_k = \hat{S}^k \bar{X}_k$ and rewrite mapping (3) as follows:

$$\bar{Y}_{k+1} = \hat{S}^{k+1} \bar{F}(\hat{S}^{-k} \bar{Y}_k). \tag{5}$$

The discrete map (5) is smooth due to the smoothness of system (1). Moreover, if system (1) has traveling-wave solutions in a form $\varphi_n(t) = \varphi(n - vt)$, then these solutions correspond to the fixed points of the map (5). In this case $t_k = k/v$ and v is the front velocity. Thus, as explained above, we expect that with variation of the system parameters these fixed points of the smooth map will lose stability through generic scenarios of codimension 1 and yield the stable propagating fronts of transition, which are not traveling waves. In the next section, this possible loss of stability of the kinks is exemplified for two well-known benchmark models.

III. EXAMPLES

A. Triparabolic potential

As the first example, we examine a model with a linear nearest-neighbor coupling $U_1(\varphi) = \varphi^2/2$ and a differentiable triparabolic on-site potential U_2. Similar potentials were previously considered in several works as a generalization of the biparabolic potential by inclusion of a nonconvex region that smoothens the cusp [31,23,3]. The third intermediate nonconvex region is often addressed as a "spinodal region."

The triparabolic potential is considered as a smoothening of the biparabolic potential with equal well curvatures ω_0^2 and the potential barrier situated at the distance $b = \sqrt{2B}/\omega_0$ from the metastable well. To smoothen the cusp and obtain the differentiable function, one introduces the spinodal region of width 2δ with appropriate matching (a plot is presented in Fig. 2):

$$U_2(\varphi) = \begin{cases} \frac{\omega_0^2 \varphi^2}{2} & \varphi < b - \delta \\ a_s \varphi^2 + b_s \varphi + c_s & b - \delta < \varphi < b + \delta, \\ \frac{\omega_0^2 (\varphi - \varphi^*)^2}{2} - Q & \varphi > b + \delta \end{cases}$$

$$a_s = \frac{1}{4} \frac{\omega_0^2 (2\delta - \varphi^*)}{\delta}, \quad b_s = \frac{\varphi^* \omega_0^2 (b - \delta)}{2\delta},$$

$$c_s = -\frac{\varphi^* \omega_0^2 (b - \delta)^2}{4\delta}, \quad \varphi^* = \frac{\sqrt{2B} + \sqrt{2(B + Q)}}{\omega_0}. \tag{6}$$

It is important to notice that B is the energetic barrier of the initial nonsmooth biparabolic potential. The actual potential barrier B^* of the triparabolic potential can be expressed as

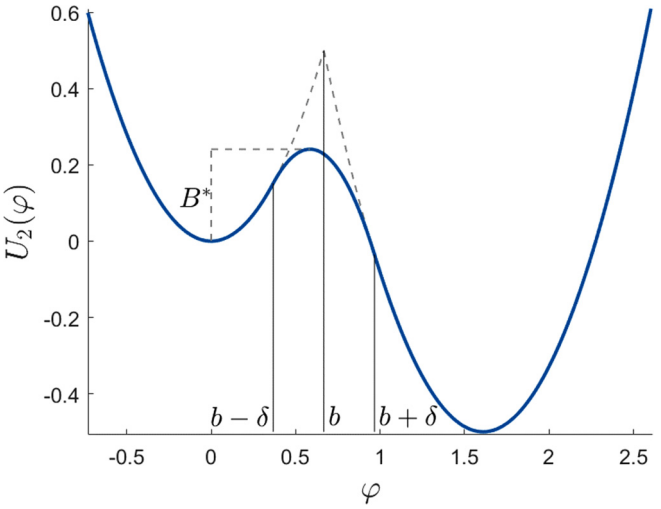

FIG. 2. Triparabolic bistable on-site potential.

$$B^* = c_s - \frac{b_s^2}{4a_s}. \tag{7}$$

The force $F_2(\varphi) = -U_2'(\varphi)$ can be expressed in symmetric form with respect to the bias force σ, which is addressed in the literature as a configurational force [21]:

$$F_2(\varphi) = \sigma + \begin{cases} f_1 & \varphi < b - \delta \\ f_2 & b - \delta < \varphi < b + \delta, \\ f_3 & \varphi > b + \delta \end{cases}$$

$$\sigma = -\frac{\omega_0}{2}[\sqrt{2B} - \sqrt{2(B + Q)}], \quad f_1 = -\omega_0^2 \varphi - \sigma,$$

$$f_2 = -a_s \varphi - b_s - \sigma, \quad f_3 = -\omega_0^2 (\varphi - \varphi^*) - \sigma. \tag{8}$$

This representation is symmetric in terms of $f_1(b - \delta) = -f_3(b + \delta)$ for any Q, whereas the term that is responsible to the drive is the configurational force σ, with the following equivalent condition for nondegeneracy: $Q \neq 0 \Leftrightarrow \sigma \neq 0$.

1. Particular case $\delta = 0$: Classical Atkinson-Cabrera model

When $\delta = 0$, the potential U_2 reduces to the well-known biparabolic on-site potential (the region $b - \delta < \varphi < b + \delta$ disappears). This model has an especially simple structure. As was mentioned above, here we consider the case of equal well curvatures. Therefore, between the instances when some particle crosses the barrier, the system is in fact linear. This simplification allows us to explore the stability of well-known kink solution [2,19–21] in explicit manner with the help of Floquet analysis.

One should explore the evolution of small perturbations of fixed points of map (5) in a linear approximation. This task requires computation of the monodromy matrix which describes the evolution of perturbation of the state vector (2), for a single period.

According to the theory, the loss of stability occurs when at least one eigenvalue leaves the unit circle in the complex plane. We select the start of the period, τ, immediately after particle $m - 1$ has passed the energetic barrier $\varphi_{m-1} = b$ and the end

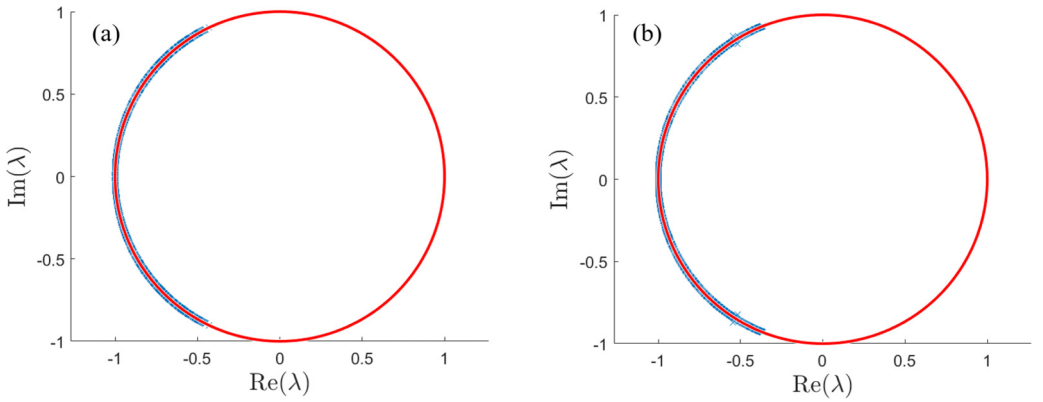

FIG. 3. Floquet multipliers at the transition from (a) stable traveling wave, $\omega_0 = 1.13$, to (b) an unstable one, $\omega_0 = 1.15$, for a model with a biparabolic bistable on-site potential. Parameters: $Q = 0.5$, $B = 0.5$, $\xi = 0$, $n = 500$, $m = 250$.

of the period—the time instance, when the particle m crosses the barrier. In the selected model, the evolution of the state vector (and, therefore, the evolution of its small perturbations) between the barrier crossings obeys a linear equation and thus does not depend on the unperturbed solution. Formally, the linear evolution of the state vector is defined by operator $\hat{A}$:

$$\dot{\bar{X}} = \hat{A}\bar{X}. \tag{9}$$

The instance when the particle crosses the barrier corresponds to a discontinuous jump of acceleration of this particle. The value of this jump depends on the unperturbed solution for the kink. The effect of such discontinuities on the evolution of small perturbations of the phase flow is conveniently taken into account with the help of so-called saltation matrices [38–41]. We denote the appropriate "saltation operator" for our infinite chain as $\hat{D}$. Thus, the monodromy operator may be formally written as follows:

$$\hat{M} = \hat{Q}\hat{D}, \quad \hat{Q} = e^{\tau\hat{A}}. \tag{10}$$

For a genuine infinite chain, the eigenvalues of the monodromy operator will not depend on the exact site at which the crossing occurs. However, for practical calculations we need to truncate the state vector and to use finite matrices instead of the operators. In the considered classical Atkinson-Cabrera model, all coupling springs have the same unit stiffness, and all on-site springs have equal stiffness ω_0^2. Therefore, the truncated matrix A of the linear evolution does not depend on the specific sites of the truncation, but only on the length of the truncated fragment of the chain. The explicit shape of this matrix is given by block construction in (11), where I is a $n \times n$ identity matrix, 0 is a $n \times n$ zero matrix, and the Laplace adjacency matrix L is presented below:

$$A_{2n\times 2n} = \begin{pmatrix} 0 & I \\ L & 0 \end{pmatrix}, \tag{11}$$

$$L_{n\times n} = \begin{pmatrix} -1-\omega_0^2 & 1 & 0 & \cdots & 0 \\ 1 & -2-\omega_0^2 & \ddots & \ddots & \vdots \\ 0 & \ddots & \ddots & \ddots & 0 \\ \vdots & \ddots & \ddots & -2-\omega_0^2 & 1 \\ 0 & \cdots & 0 & 1 & -1-\omega_0^2 \end{pmatrix}. \tag{12}$$

As for the saltation matrix, we construct it in a way that the discontinuity site is inside the truncated fragment of the chain, and not close to its boundaries. The exact meaning of these conditions will be clarified below. The saltation matrix is constructed geometrically in the phase plane in terms of the normal ν to the switching surface Σ that in our case is simply $\Sigma = \varphi_m$, f_p^-, and f_p^+, which are computed as

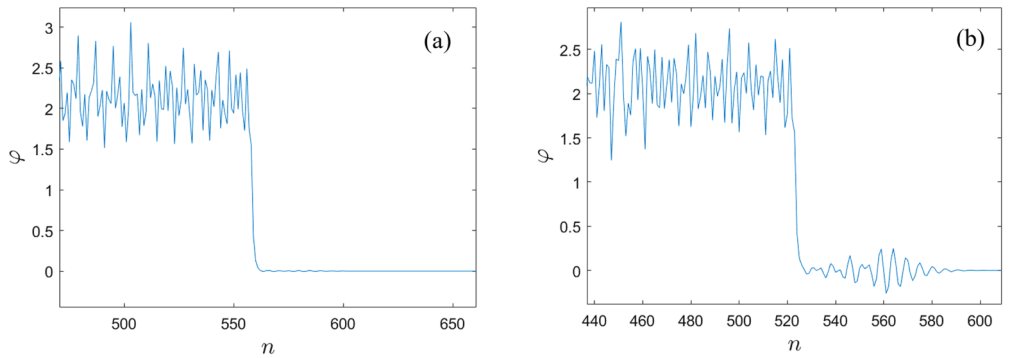

FIG. 4. Loss of stability of the traveling wave with a biparabolic bistable on-site potential; (a) $\omega_0 = 1.13$, (b) $\omega_0 = 1.15$. Common parameters: $Q = 0.5$, $B = 0.5$, $\xi = 0$, $t = 1000$.

$f_p = \dot{\tilde{X}}$ at the instances before and after crossing the barrier, respectively [38]:

$$D = I + \frac{(f_p^+ - f_p^-)v^T}{v^T f_p^- + \frac{\partial v}{\partial t}\big|_{t=t_p}}. \tag{13}$$

In our case of the acceleration discontinuity, the saltation matrix is presented by block construction in (14), where 0 is a $n \times n$ zero matrix, I is a $n \times n$ identity matrix, and C is presented below in Eq. (15). The particle that changes acceleration at the particular instance is m, and for this reason (m, m) is the only nonzero term in matrix C.

$$D_{2n\,\times\,2n} = \begin{pmatrix} I & 0 \\ C & I \end{pmatrix}, \tag{14}$$

$$C_{n\times n} = \begin{pmatrix} 0 & \cdots & 0 & 0 & 0 & \cdots & 0 \\ \vdots & \ddots & \vdots & \vdots & \vdots & \ddots & \vdots \\ 0 & \cdots & 0 & 0 & 0 & \cdots & 0 \\ 0 & \cdots & 0 & \frac{\ddot{\varphi}_m^+ - \ddot{\varphi}_m^-}{\dot{\varphi}_m^-} & 0 & \cdots & 0 \\ 0 & \cdots & 0 & 0 & 0 & \cdots & 0 \\ \vdots & \ddots & \vdots & \vdots & \vdots & \ddots & \vdots \\ 0 & \cdots & 0 & 0 & 0 & \cdots & 0 \end{pmatrix}. \tag{15}$$

The values that are required for the computation of the monodromy matrix, $\ddot{\varphi}_m^+$ (the acceleration of particle m after crossing the barrier), $\ddot{\varphi}_m^-$ (the acceleration of particle m before crossing the barrier), $\dot{\varphi}_m^-$ (the speed of particle m before crossing the barrier), and the period $\tau = 1/V$ are straightforwardly extracted from the known analytical solution [20,21]. It should

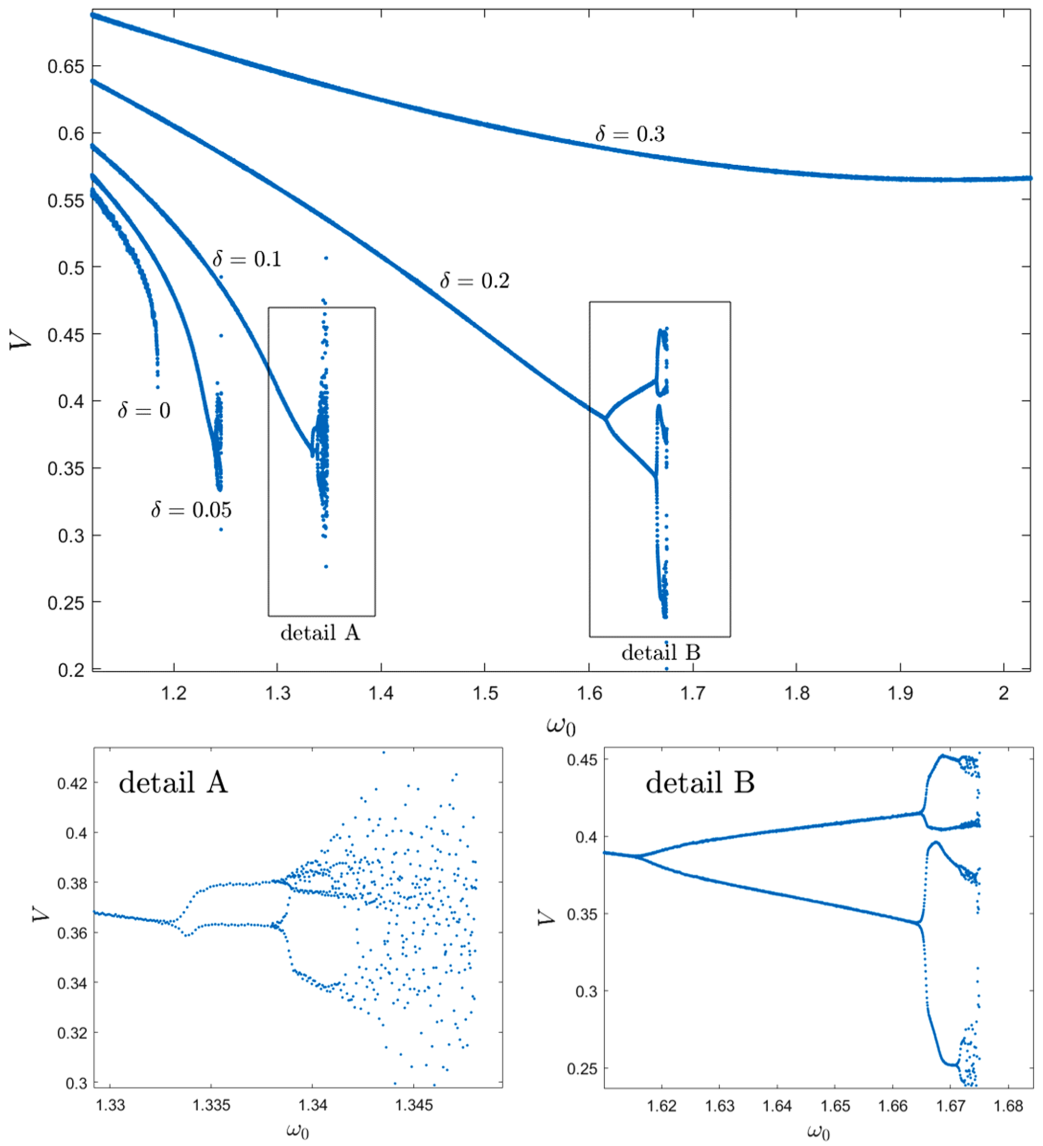

FIG. 5. Bifurcation diagram for the chain with triparabolic bistable on-site potential; Fixed parameters: $Q = 0.5$, $B = 0.5$, $\xi = 0.005$.

be stressed that this single off-diagonal term of the saltation matrix depends on the solution for the unperturbed kink and governs the loss of stability.

In the numerical simulations, the truncated length, n, is chosen to be large enough, and we check that further elongation does not affect the stability threshold. The length $n = 500$ was found to be more than sufficient for this purpose. Then, the problem becomes easy enough to be handled by a personal computer. The site of the barrier crossing, m, is chosen in the middle of the chain. Yet, it was checked that the stability thresholds are not affected in any noticeable manner by displacement of the site by 50 units in each direction.

We gradually increase the bifurcation parameter ω_0 and examine the eigenvalues of M. At $\omega_0 = 1.13$ all eigenvalues still are at the unit circle, whereas, at about $\omega_0 = 1.15$, one observes two eigenvalues that detach from the unit circle, thus indicating the loss of stability. These detaching eigenvalues are a complex conjugate, and thus one deals with Hopf bifurcation (see Fig. 3). To verify the prediction, the system is simulated numerically for the values of ω_0, which correspond to the states right before and right after the stability loss. The results are presented in Fig. 4. One observes that the loss of stability indeed occurs close to $\omega_0 = 1.15$ and is characterized by radiation on both sides of the front, in complete correspondence to the analytical predictions.

2. *Numerical study of the case* $\delta \neq 0$

To numerically examine the pattern of loss of stability for a triparabolic potential with a nondegenerate spinodal region ($\delta \neq 0$), we integrate Eq. (1) with the specified potentials U_1, U_2. For a sufficiently long chain, the transition front is initiated by applying an initial velocity to the first particle. Specifically, throughout the simulations the following condition was used, $\dot{\varphi}_1(t = 0) = 10$, though the exact magnitude was not found to influence the velocity of propagation in the steady state. In Sec. III C the effect of initial conditions is further addressed.

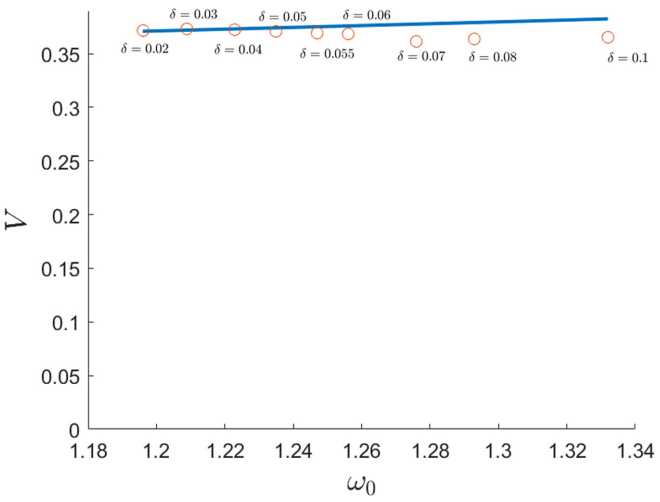

FIG. 6. Loss of stability of the traveling-wave solution with a triparabolic bistable on-site potential. Solid line: theoretical limit; circles: numerical data. Fixed parameters: $Q = 0.5, B = 0.5, \xi = 0.005$.

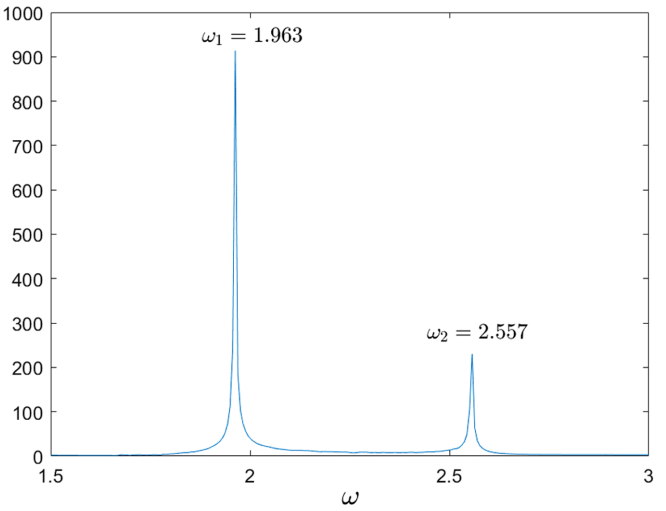

FIG. 7. FFT of a tail particle in the double-period region of the bifurcation diagram. $Q = 0.5$, $B = 0.5$, $\xi = 0.005$, $\delta = 0.2$, $\omega_0 = 1.65$.

Then one parameter is varied slowly enough to ensure an evolution that converges to the steady state of the kink at any instantaneous parameter value. The damping ($0 < \xi \ll 1$) is incorporated to stabilize the numerical solutions, and is chosen to be low enough, such that the obtained solutions can be considered as a small perturbation of the undamped case. It was verified that further decrease of the damping affected the convergence time without any noticeable effect on the bifurcation diagrams. In this example, the frequency of free oscillations in the well ω_0 is selected as the bifurcation parameter. The velocity of kink propagation V is instantaneously evaluated in the course of simulation, as the inverse of the time required for the front to pass between two neighboring sites:

$$V = V_j = (t_j - t_{j-1})^{-1}. \tag{16}$$

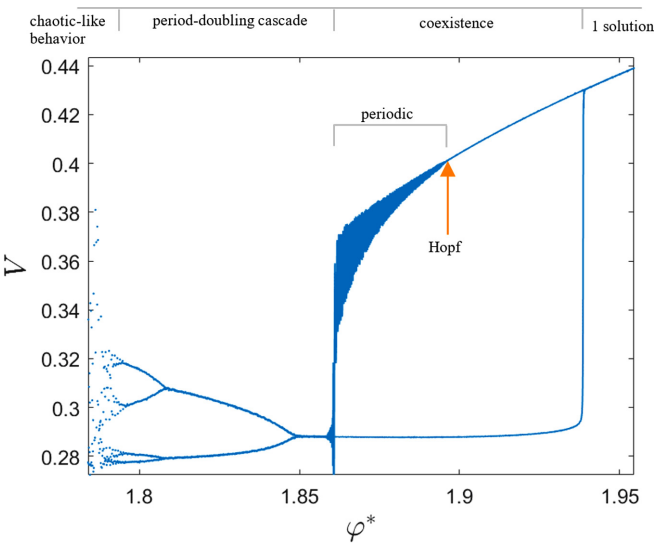

FIG. 8. Bifurcation diagram of the front velocity as a function of φ^* change. $B = 0.47$, $Q = 0.5$, $\xi = 0.02$.

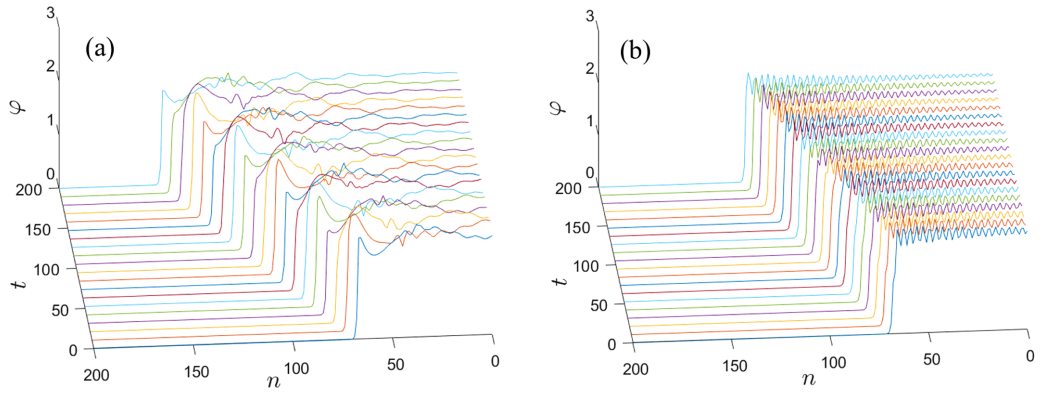

FIG. 9. Coexistence of propagating traveling waves for the same set of parameters: (a) $V = 0.404$, (b) $V = 0.2877$. Parameters: $\varphi^* = 1.9$, $Q = 0.5$, $B = 0.47$, $\xi = 0.02$.

In Fig. 5 we present a diagram for the kink velocity V as a function of bifurcation parameter ω_0. Different curves in Fig. 5 correspond to different values of δ. The left curve plotted for $\delta = 0$ corresponds to the Atkinson-Cabrera model, discussed above. As δ increases, the diagrams deviate considerably from the biparabolic case. For the triparabolic on-site potential, for all cases besides $\delta = 0$ we clearly resolve a period-doubling cascade, apparently leading to chaoticlike propagation of the kink (appears as a "scatter" of points in the plot).

As mentioned above, for the case of the traveling-wave kink one obtains $V_j = v = \text{const.}$ for all particles. The single-branch dependence of V on ω_0 implies the stability of the traveling-wave kink. Multiplication of the branches means that for the same set of parameters one records different values of V_j. Consequently, the bifurcation of the single-branch curve corresponds to the loss of stability of the traveling-wave kink.

An important question to consider is what triggers the initial loss of stability of the traveling wave. The dispersion relation within the convex wells reads

$$\omega = \sqrt{\omega_0^2 + 4\sin^2\frac{k}{2}}. \tag{17}$$

From Eq. (17) it follows that the frequency of oscillation of particles within the tail is bounded in the propagation zone:

$$\omega_0 \leqslant \omega \leqslant \omega_{tail\ \max} = \sqrt{\omega_0^2 + 4}. \tag{18}$$

We compare the propagation zone with the natural frequency related to the kink propagation in the discrete chain. The front passes the barrier with period $\tau = 1/V$ and the associated cyclic frequency is defined as follows:

$$\omega_p = \frac{2\pi}{\tau} = 2\pi V. \tag{19}$$

For the considered case, we observe the loss of stability of the traveling-wave solution, when the kink propagation frequency approaches the upper passband: $\omega_p \approx \omega_{tail\ \max}$; hence, the following *approximate* analytical criterion can be suggested for the stability of the traveling-wave kinks in the considered model:

$$V \geqslant \frac{1}{2\pi}\sqrt{\omega_0^2 + 4}. \tag{20}$$

To verify the criterion (20), we numerically determine the actual point of stability loss $(\omega_{0,cr}, V_{cr})$ for different values of δ in Fig. 6. The numerical results are in good agreement with the analytical prediction for $\delta \to 0$. This can shed light on the limit of stability of the celebrated Atkinson-Cabrera model which corresponds to $\delta = 0$, though it requires a more specific exploration in the limit $\xi \to 0$. As δ increases, the numerical results deviate from the theoretical curve. This may be explained by the influence of the spinodal zone that governs the interaction within the transitional area.

Once the stability of the traveling wave is lost, an apparently stable solution with a double spatial period of propagation

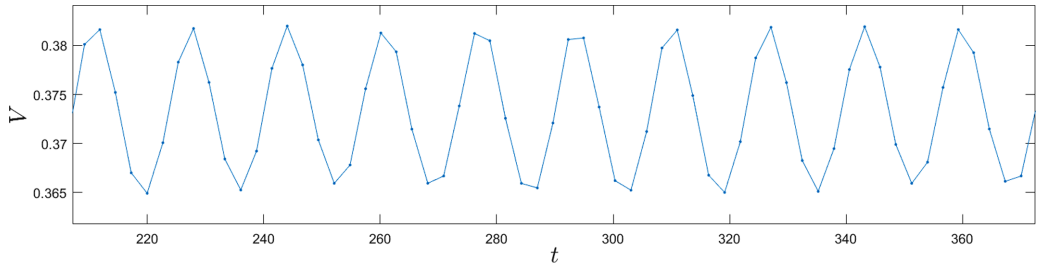

FIG. 10. An oscillatory front velocity following a Hopf bifurcation of the fast velocity branch. Parameters: $\varphi^* = 1.871$, $Q = 0.5$, $B = 0.47$, $\xi = 0.02$.

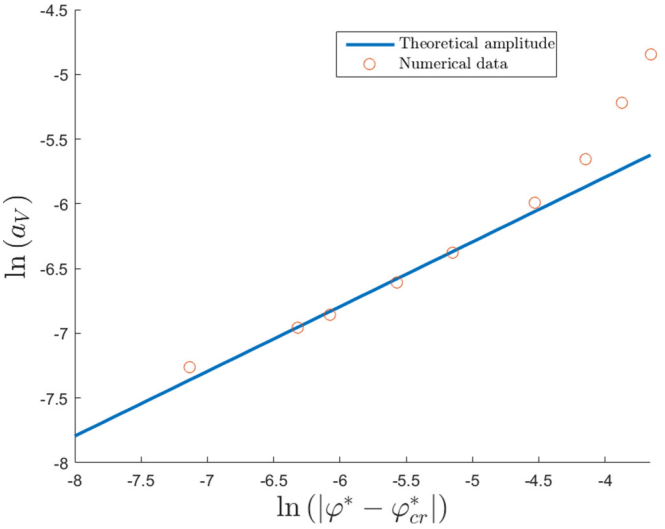

FIG. 11. Modulation amplitude of Hopf bifurcation, double logarithmic scale. Slope of the line is equal to $\frac{1}{2}$. Parameters: $\varphi^*_{cr} = 1.8958$, $\xi = 0.02$, $Q = 0.5$, $B = 0.47$.

appears. Numerical sampling within the double-period region reveals that the loss of stability results in further modifications of the solution. First, at the exact point of stability loss, an additional frequency equal to $\omega_{tail\ \max}$ appears in the spectrum of the tail particles. In total, at this instance the spectrum of the tail consists of $\omega_{tail\ \max}$ and the frequency ω in accordance with (17), with phase velocity equal to the velocity of the kink. As parameter ω_0 increases, the frequencies of the tail remain almost constant. A typical fast Fourier transform (FFT) is taken for $\delta = 0.2$, $\xi = 0.005$ and is presented in Fig. 7, which demonstrates this point. Further dynamics of the kink beyond the stability loss requires additional analysis.

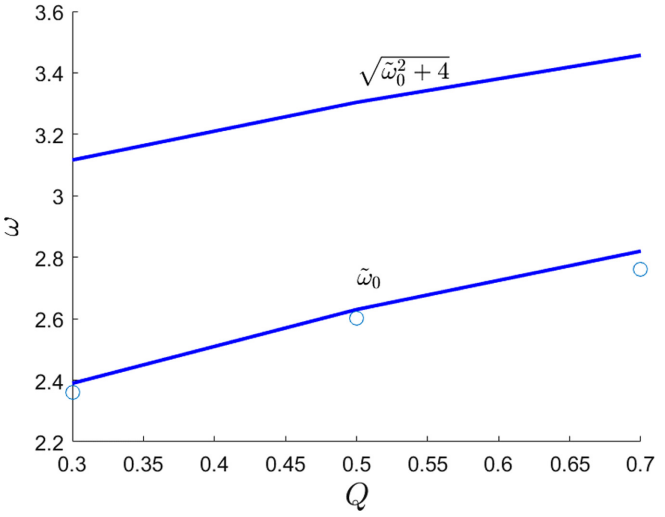

FIG. 12. Loss of stability due to Hopf bifurcation; Solid line: frequency band limits; circles: propagation frequency at stability loss. Parameters: $\xi = 0.02$, $B = 0.47$.

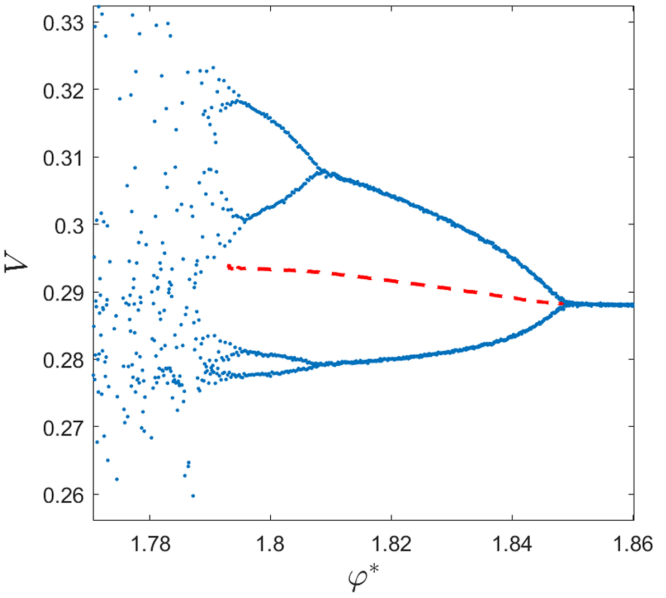

FIG. 13. Solution within the period-doubling region. Dashed red: averaged front velocity according to (22). Fixed parameters: $\xi = 0.02$, $Q = 0.5$, $B = 0.47$.

B. φ^4 potential

1. Exploration of the solutions and bifurcations

Here we consider an example of a "fully nonlinear potential"—the simple and very popular φ^4 model with linear nearest-neighbor coupling $U_1 = (\varphi_n - \varphi_{n+1})^2/2$ and quartic on-site potential $U_2(\varphi) = a_2\varphi^2 + a_3\varphi^3 + a_4\varphi^4$ with coefficients adjusted to deliver the desired values of Q, B, φ^*. Bifurcation diagrams are produced for the control parameters φ^* and Q. In the simulation, one of these parameters is varied slowly enough to ensure a front propagation that corresponds to the steady state at the instantaneous parameter. The initiation here is similar to that in Sect. III A 2. It is important to notice that for some parameters, where two solutions coexist, each solution is initiated in the region where it apparently is stable and unique and then the coexistence region is approached by numerical continuation for each solution in the appropriate

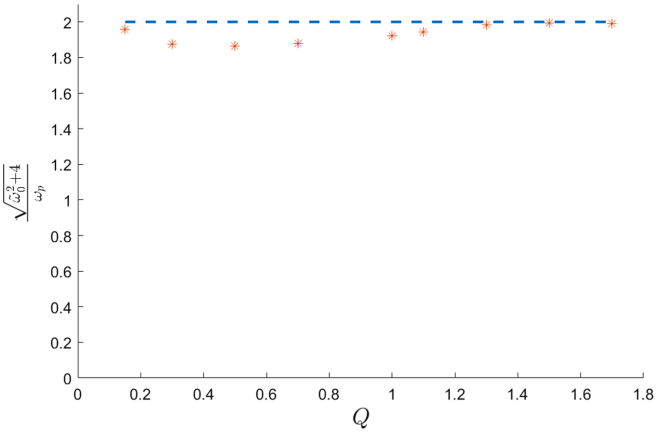

FIG. 14. Frequency ratio at the period-doubling loss of stability for the φ^4 potential. Fixed parameters: $\xi = 0.02$, $B = 0.47$.

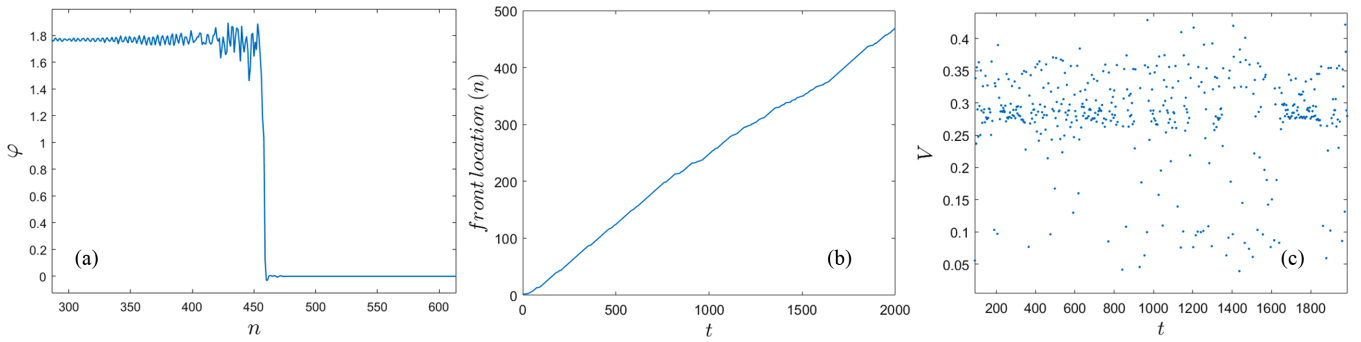

FIG. 15. Wave propagation in the chaoticlike region: (a) $\varphi = \varphi(n)$; $t = 2000$, (b) front location as a function of time, (c) front velocity as a function of time. Parameters: $\varphi^* = 1.77$, $Q = 0.5$, $B = 0.47$, $\xi = 0.02$.

direction, in order to explore the hysteretic behavior. Further comments on the initiation and stability of the solutions are presented in Sec. III C. Again, the measured quantity is the velocity of transition of the front between two neighboring sites.

First, we present the bifurcation diagram of the front velocity as a function of parameter φ^* (Fig. 8). It is important to notice that changing the parameter φ^* affects parameter a_2 that governs the frequency of free oscillations within the stale well.

One observes that for $\varphi^* > 1.94$ a single solution exists. The latter is similar to, for instance, the well-known traveling-wave fronts, which satisfy the admissibility conditions in the Atkinson-Cabrera model. In the region $1.86 < \varphi^* < 1.94$, two different solutions coexist. One is a continuation of the $\varphi^* > 1.94$ branch, while for the second, the front velocity is about 40% lower. The structure differences as well as the different rates of propagation of the two traveling-wave solutions are demonstrated in $n - t - \varphi$ space in Fig. 9. Stability of both waves was verified numerically by introducing relatively strong random perturbations (see Sec. III C for further details). The difference between the velocities is about 40%, and the frequency content considerably differs.

An additional interesting feature is that the upper branch undergoes the Hopf bifurcation at about $\varphi^* = 1.897$. Consequently, over the upper branch in the region $1.861 < \varphi^* < 1.897$, the stable propagating front violates the traveling-wave ansatz and propagates with oscillations. This phenomenon may be related to stick-slip behavior reported in similar systems [10,42]. Example of such behavior is presented in Fig. 10. In Fig. 11 we show a typical illustration for the Hopf bifurcation relationship (21) between the bifurcation parameter $|\varphi^* - \varphi^*_{cr}|$ and the modulation amplitude of V in the region of quasiperiodic propagation. The amplitude of the front oscillations starts growing as φ^* reaches the point $\varphi^* = 1.861$.

$$a_V \sim \sqrt{|\varphi^* - \varphi^*_{cr}|}. \tag{21}$$

Similarly to the previous subsection, we assume that the Hopf bifurcation is caused by certain resonance between the discrete kink frequency and the passband. To reveal this relationship, we look for the bifurcation points numerically in the $Q - \varphi^*$ plane and evaluate the frequency of propagation ω_p (19). Also, we estimate the local curvature of the stable well $\tilde{\omega}_0$ in the vicinity of its minimum as a Taylor expansion of the φ^4 potential for the particular set of parameters $B - Q - \varphi^*$. Then, the linear propagation zone obeys $\tilde{\omega}_0 < \omega < \sqrt{\tilde{\omega}_0^2 + 4}$. We show in Fig. 12 the actual loss of stability values ω_p. It turns out that in this case loss of stability occurs due to the resonance with the lower passband.

As the value of φ^* is further decreased, the front velocity enters a "period-doubling" cascade. The first doubling from a single branch to two branches occurs at $\varphi^* = 1.85$ and the lowest parameter value at which distinct branches of period doubling are observed is $\varphi^* = 1.791$, with eight branches. Within the doubling region the stationary propagation can be

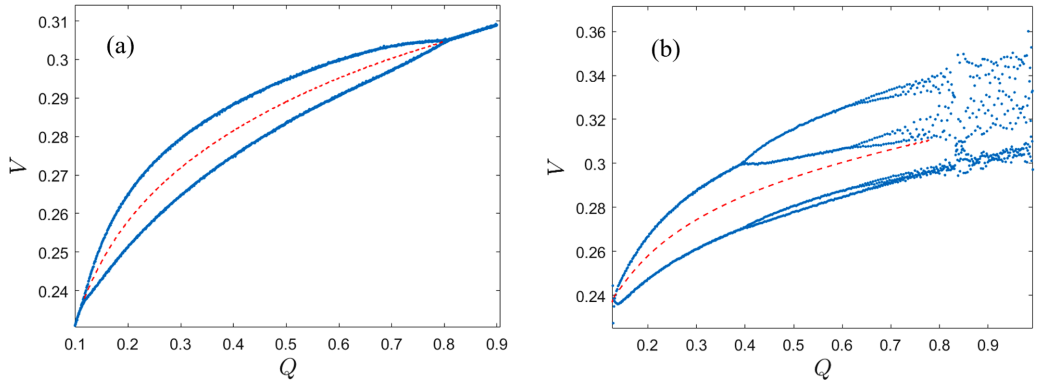

FIG. 16. Bifurcation diagram of the front velocity as a function of Q change: (a) $\varphi^* = 1.84$, (b) $\varphi^* = 1.8$. Fixed parameters: $\xi = 0.02$, $B = 0.47$. Dashed red: averaged front velocity according to (22).

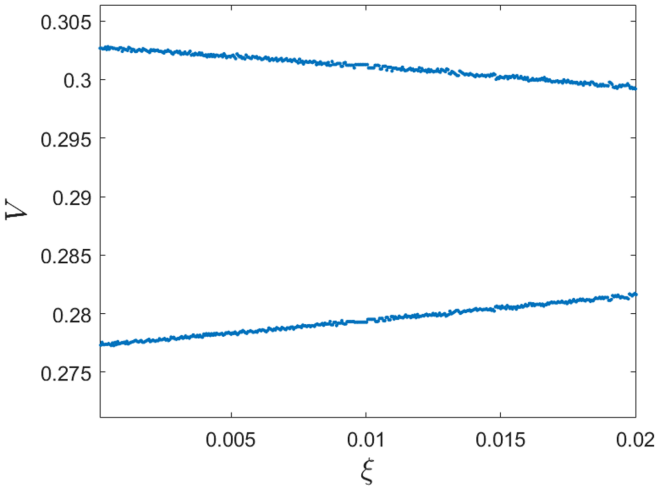

FIG. 17. Sensitivity of the solution to on-site damping change. Parameters: $\varphi^* = 1.83,\ Q = 0.5,\ B = 0.47$.

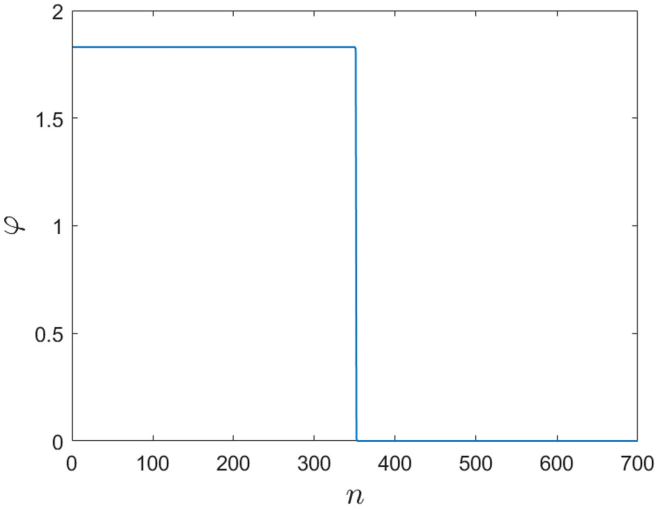

FIG. 18. Piecewise constant initiation profile.

described in an averaged sense as follows:

$$\langle V\rangle = \frac{m}{\sum_{j=1}^{m}\Delta t_j} = \frac{m}{\sum_{j=1}^{m}\frac{1}{V_j}}. \tag{22}$$

Here m is the number of branches of front velocity for the specific parameters φ^*, Q. The averaged front velocity is demonstrated in Fig. 13.

Again, it is reasonable to assume that there exists a certain resonance that triggers the entrance into the period-doubling cascade. Similarly to the previous analysis of the Hopf bifurcation, we determine the stability loss in terms of $Q - \varphi^*$ values and estimate the approximate curvature $\tilde{\omega}_0$ at each parameter set. Then ratio (23) is evaluated for different values of Q and plotted in Fig. 14. One can observe that the ratio is very close to 2 : 1 and asymptotically tends to it for high Q.

$$\frac{\omega_{tail\ \max}}{\omega_p} = \frac{\sqrt{\tilde{\omega}_0^2 + 4}}{\omega_p}. \tag{23}$$

Finally, the decrease in parameter φ^* to the region $\varphi^* < 1.79$ leads to an apparently chaotic propagation of the kink. This appears in Figs. 8 and 13 as a scatter of points, yet at each section (for each value of φ^*) it corresponds to a single nontraveling wave. More exactly, the kink propagates with certain average velocity, with chaoticlike oscillations around this average value. Figure 15 presents an example of such a response. Subplot (a) shows that visually the response shape does not deviate much from typical responses in the nonchaotic regions. However, when exploring the plots of front location (b) and front velocity (c) as a function of time, the chaos is visually evident.

In Fig. 16 additional bifurcation diagrams are presented for control parameter Q for different fixed values of φ^*. At $\varphi^* = 1.84$ the period doubling occurs at $Q = 0.11$ and a period halving at $Q = 0.81$; hence this section does not lead to the chaoticlike behavior. By taking a different section, $\varphi^* = 1.8$, as Q is increased, the periods are doubled to the total number of 16, and at about $Q = 0.78$ the response is again chaoticlike.

2. *Effect of damping*

Throughout the simulations of this subsection, the on-site damping was chosen as $\xi = 0.02$ to faster suppress effects of initial conditions that turned out to decay very slowly without the presence of damping. Here, we examine the sensitivity of the solution to damping changes. We start the simulation at $\xi = 0.02$ and gradually decrease it to zero. The result that is presented in Fig. 17 implies that the solution is only slightly modified, so, we might expect some quantitative modifications of the bifurcation diagrams due to the damping.

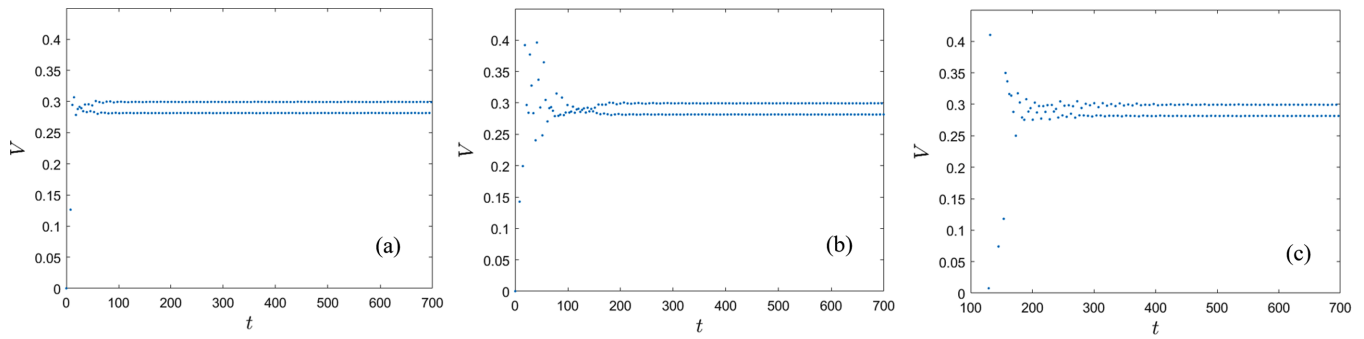

FIG. 19. Effect of initial conditions for a set of parameters with a single stable solution; (a) piecewise at $t = 0$, (b) $\dot{\varphi}_1(t = 0) = 3$, (c) $\dot{\varphi}_1(t = 0) = 50$. On-site potential: φ^4 with parameters $\varphi^* = 1.83,\ Q = 0.5,\ B = 0.47,\ \xi = 0.02$.

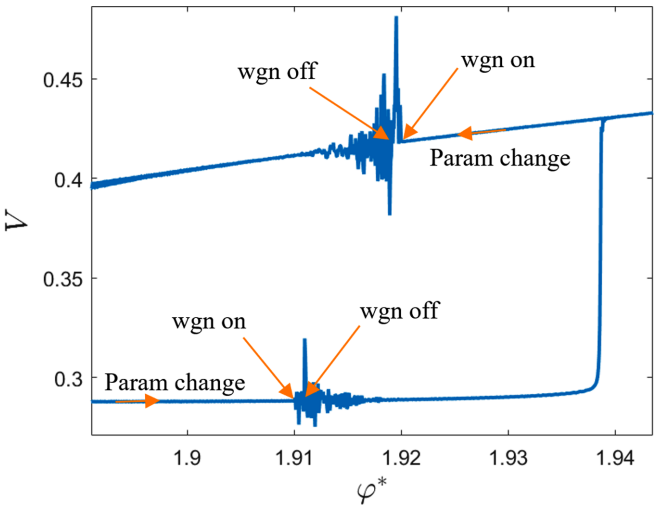

FIG. 20. Numerical stability test of coexisting solutions. On-site potential: φ^4 with parameters $\xi = 0.02$, $Q = 0.5$, $B = 0.47$.

C. Numerical exploration of the stability and sensitivity to initial conditions of the obtained solutions

Selection of initial conditions plays a key role in nonlinear systems. This is particularly crucial when the stability of solutions is examined and when several apparently stable solutions coexist with a limited basin of attraction for each one of them. Hence, in this subsection we examine how the results are affected by different perturbations of the assumed "fixed point" solutions.

We first address parameter zones where a single stable solution is assumed. Here we present an example taken for the φ^4 potential in accordance with the diagram in Fig. 8 for $\varphi^* = 1.83$ where a single solution with two periods exists. We instantiate the dynamic response in three different ways: (a) a piecewise constant profile with the left part placed within the minimum of the stable well (φ^*) and the right part within the minimum of the metastable well (Fig. 18), and (b) and (c) two initial values of velocity of the first particle: $\dot{\varphi}_1(0) = 3$, $\dot{\varphi}_1(0) = 50$. The comparison of the corresponding time series (Fig. 19) shows that all three solutions converge to the same steady state, which indicates stability of a single solution for the given set of parameters as expected. The results were similar for other combinations of parameters for both triparabolic and φ^4 potentials in the regions where a single stable solution was assumed.

In the φ^4 model a coexistence of two solutions was observed. To examine the stability of the two branches of the coexisting solutions, we perform the following numerical test. During the gradual change of parameter over each branch we turn on a white Gaussian noise over the entire chain during some interval of parameter value and then shut it off. Specifically, over the upper branch the noise is turned on at $\varphi^*{}_{\rm on} = 1.92$, and off at $\varphi^*{}_{\rm off} = 1.919$; over the lower branch the noise is turned on at $\varphi^*{}_{\rm on} = 1.91$ and off at $\varphi^*{}_{\rm off} = 1.911$. The results are shown in Fig. 20. In both cases the response is stabilized to the respective branch after a period of time (or equivalently a period of parameter change). This might indicate the stability of both coexisting solutions.

IV. CONCLUDING REMARKS

To conclude, we reveal that regular codimension 1 bifurcations of the fixed points in an appropriately defined smooth map correspond to quite unusual patterns of the transition front propagation in chains with a bistable nondegenerate on-site potential. One encounters quasiperiodic, multiperiodic, and chaoticlike propagation—all these solutions are beyond the common traveling-wave behavior. These propagation regimes can be interpreted as the propagating kinks with coupled oscillatory states.

Several mechanisms of stability loss were revealed for the considered triparabolic and φ^4 model examples. In all of the examined cases, the loss of stability was due to the resonances between the kink propagation frequency and the boundaries of the propagation zone of the oscillatory tail. However, due to the variety of possible resonances revealed [with either upper or lower limits of the passband, and either 1:1 or 2:1 frequency ratio] such interactions turn out to be substantially model dependent. For the Atkinson-Cabrera model, one can obtain explicit semianalytic evaluation of the stability threshold with the help of a relatively simple approach based on linear algebra, instead of heavy direct numeric calculation of the monodromy matrix. In this model, the loss of stability of the traveling-wave kink occurs far above the limit of the admissibility conditions. From a physical point of view, after the loss of stability one still observes the propagating transition front with an oscillatory tail. However, this solution does not obey the traveling-wave ansatz, the oscillatory tail has a complicated structure, and the kink velocity is constant only on average.

It is well known that, for instance, for the celebrated continuous degenerate φ^4 model one encounters oscillatory states around the stable kink solutions [43]. However, in the considered system the situation is substantially different: The kinks with coupled periodic or chaotic oscillatory states can propagate through the lattice in the regions of the parametric space where the kinks without such coupled states do not exist or are unstable. Formation of a discrete breather attached to the kink has been reported also in a driven Frenkel-Kontorova chain [24].

The last remark is that the observed regularities follow only from the general properties of map (5). One can expect that the regimes of front propagation beyond the common traveling waves will be ubiquitous in similar lattice models, both in one dimension and in higher dimensions.

ACKNOWLEDGMENT

The authors are very grateful to the Israel Science Foundation (Grant No. 1696/17) for financial support.

[1] Y. I. Frenkel and T. Kontorova, On the theory of plastic deformation and twinning, Phys. Z. Sowjetunion **13**, 1 (1938).

[2] W. Atkinson and N. Cabrera, Motion of a Frenkel–Kontorova dislocation in a one-dimensional crystal, Phys. Rev. **138**, A763 (1965).

[3] A. Vainchtein, Effect of nonlinearity on the steady motion of a twinning dislocation, Phys. D (Amsterdam, Neth.) **239**, 1170 (2010).

[4] M. L. Floria and J. J. Mazo, Dissipative dynamics of the Frenkel-Kontorova model, Adv. Phys. **45**, 505 (1996).

[5] L. Truskinovsky and A. Vainchtein, Kinetics of martensitic transitions: Lattice model, SIAM J. Appl. Math. **66**, 533 (2005).

[6] D. A. Bruce, Scattering properties of ferroelectric domain walls, J. Phys. C **14**, 5195 (1981).

[7] L. I. Slepyan, Dynamics of a crack in a lattice, Sov. Phys. Dokl. **26**, 538 (1981).

[8] A. M. Balk, A. V. Cherkaev, and L. I. Slepyan, Dynamics of chains with non-monotone stress–strain relations. I. Model and numerical experiments, J. Mech. Phys. Solids **49**, 131 (2001).

[9] M. Suezawa and K. Sumino, Lattice distortion and the effective shear modulus along a coherent twin boundary, Phys. Status Solidi A **36**, 263 (1976).

[10] M. Weiss and F. J. Elmer, Dry friction in the Frenkel-Kontorova-Tomlinson model: Dynamical properties, Z. Phys. B: Condens. Matter **104**, 55 (1997).

[11] D. R. Nelson, *Defects and Geometry in Condensed Matter* (Cambridge University Press, Cambridge, 2002).

[12] A. S. Kovalev, A. D. Kondratyuk, A. M. Kosevich, and A. I. Landau, Theoretical description of the crowdion in an anisotropic crystal based on the Frenkel-Kontorova model including and elastic three-dimensional medium, Phys. Status Solidi B **177**, 117 (1993).

[13] A. Carpio, L. L. Bonilla, and G. Dell'Acqua, Motion of wave fronts in semiconductor superlattices, Phys. Rev. E **64**, 036204 (2001).

[14] F. Fraternali, T. Blesgen, A. Amendola, and C. Daraio, Multiscale mass-spring models of carbon nanotube foams, J. Mech. Phys. Solids **59**, 89 (2011).

[15] E. Bichoutskaia, M. I. Heggie, Yu. E. Lozovik, and A. M. Popov, Multi-walled nanotubes: Commensurate-incommensurate phase transition and NEMS applications, Fullerenes, Nanotubes Carbon Nanostruct. **14**, 131 (2006).

[16] A. R. Bishop, Nonlinear collective excitations in superionic conductors, J. Phys. C: Solid State Phys. **11**, L329 (1978).

[17] J. P. Keener and J. Sneyd, *Mathematical Physiology* (Springer, New York, 1998).

[18] O. M. Braun and Y. S. Kivshar, Nonlinear dynamics of the Frenkel-Kontorova model, Phys. Rep. **306**, 1 (1998).

[19] A. Carpio and L. L. Bonilla, Oscillatory wave fronts in chains of coupled nonlinear oscillators, Phys. Rev. E **67**, 056621 (2003).

[20] I. B. Shiroky and O. V. Gendelman, Propagation of transition front in bistable nondegenerate chains: Model dependence and universality, J. Mech. Phys. Solids **104**, 144(2017).

[21] O. Kresse and L. Truskinovsky, Mobility of lattice defects: Discrete and continuum approaches, J. Mech. Phys. Solids **51**, 1305 (2003).

[22] Y. Y. Earmme and J. H. Weiner, Dislocation dynamics in the modified Frenkel–Kontorova model, J. Appl. Phys. **48**, 3317 (1977).

[23] P. Rosakis and A. Vainchtein, New solutions for slow moving kinks in a forced Frenkel–Kontorova chain, J. Nonlinear Sci. **23**, 1089 (2012).

[24] O. Braun, B. Hu, and A. Zeltser, Driven kink in the Frenkel-Kontorova model, Phys. Rev. E **62**, 4235 (1999).

[25] I. B. Shiroky and O. V. Gendelman, Propagation of transition front in nonlinear chains with non-degenerate on-site potential, Chaos **28**, 023104 (2018).

[26] N. Nadkarni, A. F. Arrieta, C. Chong, D. Kochmann, and C. Daraio, Unidirectional Transition Waves in Bistable Lattices, Phys. Rev. Lett. **116**, 244501(2016).

[27] N. Nadkarni, C. Daraio, R. Abeyarante, and M. Kochmann, Universal energy transport law for dissipative and diffusive phase transitions, Phys. Rev. B **93**, 104109 (2016).

[28] V. V. Smirnov, O. V. Gendelman, and L. I. Manevitch, Front propagation in a bistable system: How the energy is released, Phys. Rev. E **89**, 050901(R) (2014).

[29] N. Flytzanis, S. Crowley, and V. Celli, High velocity dislocation motion and interatomic force law, J. Phys. Chem. Solids **38**, 539 (1977).

[30] M. Peyrard and M. D. Kruskal, Kink dynamics in the highly discrete sine-Gordon system, Phys. D (Amsterdam, Neth.) **14**, 88 (1984).

[31] A. Vainchtein, The role of spinodal region in the kinetics of lattice phase transitions, J. Mech. Phys. Solids **58**, 227 (2010).

[32] M. Radulescu and J. Tang, Nonlinear Dynamics of Self-Sustained Supersonic Reaction Waves: Fickett's Detonation Analogue, Phys. Rev. Lett. **107**, 164503 (2011).

[33] W. Fickett, Detonation in miniature, Am. J. Phys. **47**, 1050 (1979).

[34] A. Kasimov and L. Faria, Model for Shock Wave Chaos, Phys. Rev. Lett. **110**, 104104 (2013).

[35] J. Guckenheimer and P. Holmes, *Nonlinear Oscillators, Dynamical Systems, and Bifurcations of Vector Fields* (Springer, New York, 1997).

[36] S. Wiggins, *Introduction to Applied Nonlinear Dynamical Systems and Chaos* (Springer, New York, 1990).

[37] T. Melvin, A. Champneys, P. Kevrekidis, and J. Cuevas, Traveling solitary waves in the discrete Schroedinger equation with saturable nonlinearity: Existence, stability and dynamics, Phys. D (Amsterdam, Neth.) **237**, 551 (2008).

[38] M. Bernardo, C. Budd, A. R. Champneys, and P. Kowalczyk, *Piecewise-smooth Dynamical Systems: Theory and Applications* (Springer, New York, 2008).

[39] I. B. Shiroky and O. V. Gendelman, Discrete breathers in an array of self-excited oscillators: Exact solutions and stability, Chaos **26**, 103112 (2016).

[40] O. V. Gendelman, Exact solutions for discrete breathers in a forced-damped chain, Phys. Rev. E **87**, 062911 (2013).

[41] N. Perchikov and O. V. Gendelman, Dynamics and stability of a discrete breather in a harmonically excited chain with vibro-impact on-site potential, Phys. D (Amsterdam, Neth.) **292–293**, 8 (2015).

[42] A. Vanossi, N. Manini, M. Urbakh, S. Zapperi, and E. Tosatti, Colloquium: Modeling friction: From nanoscale to mesoscale, Rev. Mod. Phys. **85**, 529 (2013).

[43] T. Dauxois and M. Peyrard, *Physics of Solitons* (Cambridge University Press, Cambridge, 2006).